

Dark Matter Results from 225 Live Days of XENON100 Data

E. Aprile,¹ M. Alfonsi,² K. Arisaka,³ F. Arneodo,⁴ C. Balan,⁵ L. Baudis,⁶ B. Bauermeister,⁷ A. Behrens,⁶ P. Beltrame,³ K. Bokeloh,⁸ E. Brown,⁸ G. Bruno,⁴ R. Budnik,¹ J. M. R. Cardoso,⁵ W.-T. Chen,⁹ B. Choi,¹ D. Cline,³ A. P. Colijn,² H. Contreras,¹ J. P. Cussonneau,⁹ M. P. Decowski,² E. Duchovni,¹⁰ S. Fattori,⁷ A. D. Ferella,⁶ W. Fulgione,¹¹ F. Gao,¹² M. Garbini,¹³ C. Ghag,³ K.-L. Giboni,¹ L. W. Goetzke,¹ C. Grignon,⁷ E. Gross,¹⁰ W. Hampel,¹⁴ F. Kaether,¹⁴ H. Kettling,⁸ A. Kish,⁶ J. Lamblin,⁹ H. Landsman,¹⁰ R. F. Lang,^{15,1} M. Le Calloch,⁹ C. Levy,⁸ K. E. Lim,¹ Q. Lin,¹² S. Lindemann,¹⁴ M. Lindner,¹⁴ J. A. M. Lopes,⁵ K. Lung,³ T. Marrodán Undagoitia,⁶ F. V. Massoli,¹³ A. J. Melgarejo Fernandez,^{1,*} Y. Meng,³ A. Molinaro,¹¹ E. Nativ,¹⁰ K. Ni,¹² U. Oberlack,^{7,16} S. E. A. Orrigo,⁵ E. Pantic,³ R. Persiani,¹³ G. Plante,¹ N. Priel,¹⁰ A. Rizzo,¹ S. Rosendahl,⁸ J. M. F. dos Santos,⁵ G. Sartorelli,¹³ J. Schreiner,¹⁴ M. Schumann,^{6,†} L. Scotto Lavina,⁹ P. R. Scovell,³ M. Selvi,¹³ P. Shagin,¹⁶ H. Simgen,¹⁴ A. Teymourian,³ D. Thers,⁹ O. Vitells,¹⁰ H. Wang,³ M. Weber,¹⁴ and C. Weinheimer⁸

(The XENON100 Collaboration)

¹*Physics Department, Columbia University, New York, NY 10027, USA*

²*Nikhef and the University of Amsterdam, Science Park, Amsterdam, Netherlands*

³*Physics & Astronomy Department, University of California, Los Angeles, USA*

⁴*INFN, Laboratori Nazionali del Gran Sasso, Assergi, 67100, Italy*

⁵*Department of Physics, University of Coimbra, R. Larga, 3004-516, Coimbra, Portugal*

⁶*Physics Institute, University of Zürich, Winterthurerstr. 190, CH-8057, Switzerland*

⁷*Institut für Physik, Johannes Gutenberg Universität Mainz, 55099 Mainz, Germany*

⁸*Institut für Kernphysik, Wilhelms-Universität Münster, 48149 Münster, Germany*

⁹*SUBATECH, Ecole des Mines de Nantes, CNRS/In2p3, Université de Nantes, 44307 Nantes, France*

¹⁰*Department of Particle Physics and Astrophysics, Weizmann Institute of Science, 76100 Rehovot, Israel*

¹¹*University of Torino and INFN-Torino, Torino, Italy*

¹²*Department of Physics, Shanghai Jiao Tong University, Shanghai, 200240, China*

¹³*University of Bologna and INFN-Bologna, Bologna, Italy*

¹⁴*Max-Planck-Institut für Kernphysik, Saupfercheckweg 1, 69117 Heidelberg, Germany*

¹⁵*Department of Physics, Purdue University, West Lafayette, IN 47907, USA*

¹⁶*Department of Physics and Astronomy, Rice University, Houston, TX 77005 - 1892, USA*

We report on a search for particle dark matter with the XENON100 experiment, operated at the Laboratori Nazionali del Gran Sasso (LNGS) for 13 months during 2011 and 2012. XENON100 features an ultra-low electromagnetic background of $(5.3 \pm 0.6) \times 10^{-3}$ events $(\text{kg day keV}_{\text{ee}})^{-1}$ in the energy region of interest. A blind analysis of 224.6 live days \times 34 kg exposure has yielded no evidence for dark matter interactions. The two candidate events observed in the pre-defined nuclear recoil energy range of 6.6–30.5 keV_{nr} are consistent with the background expectation of (1.0 ± 0.2) events. A Profile Likelihood analysis using a 6.6–43.3 keV_{nr} energy range sets the most stringent limit on the spin-independent elastic WIMP-nucleon scattering cross section for WIMP masses above 8 GeV/ c^2 , with a minimum of 2×10^{-45} cm² at 55 GeV/ c^2 and 90% confidence level.

PACS numbers: 95.35.+d, 14.80.Ly, 29.40.-n,

Keywords: Dark Matter, Direct Detection, Xenon

Astronomical and cosmological observations indicate that a large amount of the energy content of the Universe is made of dark matter [1]. Particle candidates under the generic name of Weakly Interacting Massive Particles (WIMPs) [2] arise naturally in many theories beyond the Standard Model of particle physics, such as supersymmetry, universal extra dimensions, or little Higgs models. The search for these particles continues with a variety of experimental approaches [3]. In direct detection experiments, one attempts to observe the nuclear recoils (NRs) produced by WIMP scattering off nucleons [4]. The expected signal features a recoil spectrum which falls exponentially with energy and extends to a few tens of keV only. The expected low event rate requires large detectors built from radio-pure materials and

that are capable of identifying and rejecting backgrounds from various sources.

The XENON100 experiment, described in detail in [5], uses liquid xenon (LXe) as both WIMP target and detection medium, with simultaneous measurement of the ionization and scintillation signals produced by particle interactions in the active volume. The detector is a cylindrical two-phase (gas/liquid) time projection chamber (TPC) enclosing a LXe target mass of 62 kg. An additional 99 kg of the same high-purity LXe, optically separated from the target volume, is instrumented as an active scintillator veto. The TPC and the veto are mounted in a double-walled stainless-steel cryostat, enclosed by a passive shield made from OFHC copper, polyethylene, lead, and water/polyethylene. The shield is permanently

purged with boil-off N_2 gas in order to suppress radon backgrounds. The LXe is kept at the operating temperature of about -91°C by a pulse tube refrigerator (PTR) mounted outside the shield. For the run leading to this new result the PTR has been in continuous operation for a total of ~ 20 months. This is the first demonstration, to our knowledge, of a LXe detector operated over such a long period of time.

The key feature of the XENON100 TPC is its ability to reconstruct the energy and three-dimensional coordinates on an event-by-event basis. This enables background reduction by fiducial volume optimization, exploiting the self-shielding of LXe. An energy deposition in the TPC produces both ionization electrons and scintillation photons. The electrons, moved from the interaction point by a drift field of 530 V/cm , are extracted from the liquid and accelerated in the gas by a $\sim 12\text{ kV/cm}$ field, producing proportional scintillation light. The amplified charge signal (S2) and the direct scintillation signal (S1) are both detected by two arrays of $1''$ -square Hamamatsu R8520-AL photomultipliers (PMTs), selected for low radioactivity and high quantum efficiency [5]. One array is immersed in the LXe below the cathode of the TPC for optimal light collection, and one is placed in the xenon gas above the amplification gap.

The z -position of a particle interaction in the TPC is reconstructed, with a precision of 0.3 mm (1σ), from the time difference between the S1 and S2 signals and the known electron drift velocity. The localized distribution of the S2 signal over the top PMTs is used to obtain the (x, y) -coordinates using a Neural Network algorithm with an uncertainty $< 3\text{ mm}$ (1σ) [5, 6]. The spatial reconstruction also allows for the rejection of multiple-scatter events, such as from neutrons, since WIMPs are expected to interact only once. Double-scatter events can be separated when their vertices differ by $\Delta z > 3\text{ mm}$. Finally, the ratio S2/S1 is different for NRs (WIMPs, neutrons) and electronic recoils (ER; β/γ -background) and is also used for background discrimination.

XENON100 is installed at the Laboratori Nazionali del Gran Sasso (LNGS) of INFN, Italy, at an average depth of 3600 m water equivalent, where the muon flux is suppressed by 10^6 [7]. Due to careful material selection [8] and detector design [5], the total ER background of XENON100 is $\sim 5 \times 10^{-3}\text{ events} \times (\text{keV}_{\text{ee}} \times \text{kg} \times \text{day})^{-1}$ ($\text{keV}_{\text{ee}} = \text{keV}$ electron-equivalent [9]) in the dark matter energy region, before S2/S1 discrimination.

Compared to the data reported in [6], the new dark matter search is characterized by a considerably larger exposure and a substantial reduction of the intrinsic background from ^{85}Kr by cryogenic distillation. The ^{85}Kr concentration in Xe has been lowered to $(19 \pm 4)\text{ ppt}$, as measured in a Xe gas sample from the detector using ultra-sensitive rare gas mass spectrometry combined with a sophisticated Kr/Xe separation technique. This is consistent with the $(18 \pm 8)\text{ ppt}$ derived from

counting the number of delayed β - γ coincidences associated with the ^{85}Kr beta decay, assuming a $^{85}\text{Kr}/^{84}\text{Kr}$ ratio of 2×10^{-11} [10].

The data have been acquired under improved electronic noise conditions and the hardware trigger was changed to a majority design to allow for a reduced S2 trigger threshold of $> 99\%$ for S2 signals above $150\text{ photoelectrons (PE)}$. This has been directly measured using the method described in [5, 11] and leads to virtually no loss of events in the energy region of interest.

The non-uniform light collection by the two PMT arrays and the attenuation of the ionization signal by residual impurities over the maximum drift gap of 30 cm lead to a position-dependent S1 and S2 signal response. The signals are corrected using maps derived from calibration data. The S1 light yield is 3-dimensionally corrected in cylindrical coordinates (r, θ, z) in order to optimize the response very close to the PMTs. The electron lifetime τ_e [5], used to describe the ionization loss by impurities in LXe, was measured regularly with a ^{137}Cs source throughout the data taking period. The value increased from $374\text{ }\mu\text{s}$ to $611\text{ }\mu\text{s}$, with the average being $\tau_e = 514\text{ }\mu\text{s}$. The measured drift time t_d is used to correct the S2 signal size for these losses, and an additional correction in (x, y) accounts for variations due to photon collection efficiency and small inhomogeneities in the mesh electrodes. The width of the S2 signal is also corrected in (x, y, t_d) such that it is independent of these inhomogeneities. For the analysis presented here, the maximum size of the latter two corrections is 15% and 3% , respectively. The corrections, including one due to the imperfect drift field, are described in more detail [5]. The considerably larger amount of ER and NR calibration data taken during this dark matter run (48.0 and 2.7 live days, respectively), allowed for the improvement of the accuracy of most of these corrections at the percent-level.

As in the previous analysis, it was decided a priori to use the Profile Likelihood (PL) statistical inference as introduced in [12]. Both the signal and the background-only hypothesis are tested. An analysis based on the maximum gap method [13] with a pre-defined signal region (benchmark region), is used as a cross check.

The energy scale for NRs is derived from the S1 signal using the independently measured relative scintillation efficiency \mathcal{L}_{eff} via the relation $E_{\text{nr}} = (S1/L_y)(1/\mathcal{L}_{\text{eff}})(S_{\text{ee}}/S_{\text{nr}})$ (see [14] and references therein). The \mathcal{L}_{eff} parametrization of [6] is used. A hard cut in the S1 acceptance (see Fig. 1) removes nearly all events below the last measured \mathcal{L}_{eff} datapoint at 3 keV_{nr} , making the extrapolation to lower E_{nr} irrelevant. The factors $S_{\text{ee}} = 0.58$ and $S_{\text{nr}} = 0.95$ describe the scintillation quenching due to the electric field and are taken from [15]. $L_y = (2.28 \pm 0.04)\text{ PE/keV}_{\text{ee}}$ is the updated response to 122 keV gamma rays as determined from calibration measurements using lines above and below this value. The interpolation between these lines is performed

using the NEST model for scintillation [16].

After verification that the S1 pulses are not affected by electronic noise, the lower energy threshold used for this analysis was set to 3 PE, corresponding to 6.6 keV_{nr}. The PL analysis takes into account the expected WIMP energy distribution and would not need an upper energy threshold, but for practical purposes, a high threshold of 43.3 keV_{nr} (30 PE) was employed. The benchmark region is limited to an upper threshold of 30.5 keV_{nr} (20 PE) chosen to optimize the signal-to-background ratio. Signal (NR) and background (ER) events can be distinguished by their different S2/S1 ratio, where only the S2 signal detected by the bottom PMTs, S2_b, is used since it requires smaller corrections [5]. The mean of the log₁₀(S2_b/S1) band from ER calibration data is subtracted in order to remove the energy-dependence of this discrimination parameter.

The dark matter data used for this analysis were accumulated over a period of 13 months between February 28, 2011 and March 31, 2012. Besides 3 interruptions due to equipment maintenance, the data were acquired continuously. Dark matter data taking was otherwise only interrupted by regular calibrations using blue LED light (for the PMT response), a ¹³⁷Cs source (for monitoring of the LXe purity), and ⁶⁰Co and ²³²Th sources (for ER background calibration). Overall, the duty cycle of XENON100 during this dark matter run was 81%. To calibrate the response to NRs, data from an ²⁴¹AmBe neutron source were taken just before the start and right after the end of the run. The two measurements are in good agreement.

Periods with with increased electronic noise or very localized light emission in the *xy*-plane were removed from the data, as well as periods in which crucial detector parameters such as temperature or pressure fluctuated outside of their normal range. This results in a final dark matter dataset of 224.6 live days. In order to avoid analysis bias, the dark matter data was blinded from 2-100 PE in S1 by keeping only the upper 90% of the ER band, thereby masking more than 90% of the signal region.

In order to identify valid NR candidate events with the highest possible acceptance, several classes of cuts and event selections are applied to the data. Their acceptance is evaluated on NR calibration data, with the exception of quality cuts which might have a time dependence due to changing detector conditions. These are tested on the non-blind part of the science data or on the ER calibration data. The first class of cuts are basic data quality cuts which remove events that show either unidentified peaks or an excessive level of electronic noise or light (as from a very high energy event or a high voltage discharge). Since only single-scatter events are expected from WIMP interactions, the second class of cuts identifies such events using the number of S1 and S2 peaks in the waveform and the information from the active veto. Conditions on the size of the S2 and the

requirement that at least two PMTs must observe an S1 peak ensure that only data above the threshold and well above the noise level are considered. Finally, it is verified that several quantities associated with the event are consistent, e.g., that the width of the S2 signal, affected by electron diffusion in the LXe, is consistent with the *z*-position derived from the time difference between the S1 and the S2.

The acceptance of most of the cuts is given versus the size of the measured S1 signal, used to infer the NR energy scale. This is subject to large Poisson fluctuations due to the low number of quanta involved. Only the acceptance of the S2 threshold condition, S2>150 PE, is given vs. the S1 signal before Poisson-smearing since the S2 signal fluctuates independently from the S1 after the initial energy deposition. This quantity is not accessible through a direct measurement and has been numerically deconvoluted from measured data [11]. It leads to an acceptance which depends on the recoil energy spectrum once converted into the observed S1 signal (see Fig. 2 of [6]). The cuts and their acceptance determination are identical or similar to those described in [11] with the exception of the cut against electronic noise which has been improved considerably. The acceptances are shown in Fig. 1.

The fiducial volume used in this analysis contains 34 kg of LXe. The volume was determined by maximizing the sensitivity of this run given the accessible ER background above the blinding cut. The ellipsoidal shape was optimized on ER calibration data, also taking into account event leakage into the signal region. A benchmark WIMP search region to quantify the background expectation and to be used for the maximum gap analysis was defined from 6.6-30.5 keV_{nr} (3-20 PE) in energy, by an upper 99.75% ER rejection line in the discrimina-

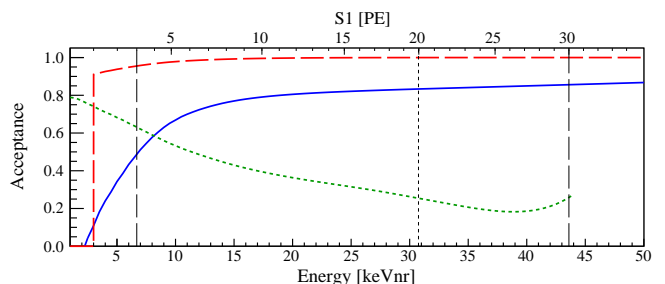


FIG. 1: Combined cut acceptance (solid blue). The S2 threshold cut S2> 150 PE (dashed red) is independent of possible fluctuations in S1 and has to be applied to the S1 spectrum before taking into account the S1 resolution. It is conservatively set to zero below 1 PE. For the cross-check with the maximum gap method [13], a hard discrimination cut is used. Its acceptance to NRs is shown by the dotted green line. The lower analysis threshold is 6.6 keV_{nr} (3 PE) and extends to 43.3 keV_{nr}, whereas the cross-check is restricted to 30.5 keV_{nr} (dashed and dotted black lines).

tion parameter space, and by the lines corresponding to $S2 > 150$ PE and a lower line at $\sim 97\%$ acceptance from neutron calibration data (see lines in Fig. 2, top).

Both NR and ER interactions contribute to the expected background for the WIMP search. The first is determined from Monte Carlo simulations, using the measured intrinsic radioactive contamination of all detector and shield materials [8] to calculate the neutron background from (α, n) and spontaneous fission reactions, as well as from muons, taking into account the muon energy and angular dependence at LNGS. The expectation from these neutron sources is $(0.17^{+0.12}_{-0.07})$ events for the given exposure and NR acceptance in the benchmark region. About 70% of the neutron background is muon-induced.

ER background events originate from radioactivity of the detector components and from β and γ activity of intrinsic radioactivity in the LXe target, such as ^{222}Rn and ^{85}Kr . The latter background is most critical since it cannot be reduced by fiducialization. Hence, for the dark matter search reported here, a major effort was made to reduce the ^{85}Kr contamination which affected the sensitivity of the previous search [6]. To estimate the total ER background from all sources, the ^{60}Co and ^{232}Th calibration data is used, with >35 times more statistics in the relevant energy range than in the dark matter data. The calibration data is scaled to the dark matter exposure by normalizing it to the number of events seen above the blinding cut in the energy region of interest. The majority of ER background events is Gaussian distributed in the discrimination parameter space, with a few events leaking anomalously into the NR band. These anomalous events can be due to double scatters with one energy deposition inside the TPC and another one in a charge insensitive region, such that the prompt S1 signal from the two scatters is combined with only one charge signal S2. Calibration data show that anomalous leakage is most likely below ~ 8 PE. The ER background estimate including Gaussian and anomalous events is (0.79 ± 0.16) in the benchmark region, leading to a total background expectation of (1.0 ± 0.2) events.

The background model used in the PL analysis employs the same assumptions and input spectra from MC and calibration data. Its validity has been confirmed prior to unblinding on the high-energy sideband and on the vetoed data from 6.6–43.3 keV_{nr}. However, the model does not include a population with $S2/S1$ values below the NR signal region extending down to the lowest energies with $S2 < 150$ PE. This population was found only after unblinding and might contribute to the background at low S1.

After unblinding, two events were observed in the benchmark WIMP search region, see Fig. 2. With energies of 7.1 keV_{nr} (3.3 PE) and 7.8 keV_{nr} (3.8 PE) both fall into the lowest PE bin used for this analysis. The waveforms for both events are of high quality and their $S2/S1$ value is at the lower edge of the NR band from

neutron calibration. There are no leakage events below 3 PE. The PL analysis yields a p -value of $\geq 5\%$ for all WIMP masses for the background-only hypothesis indicating that there is no excess due to a dark matter signal. The probability that the expected background in

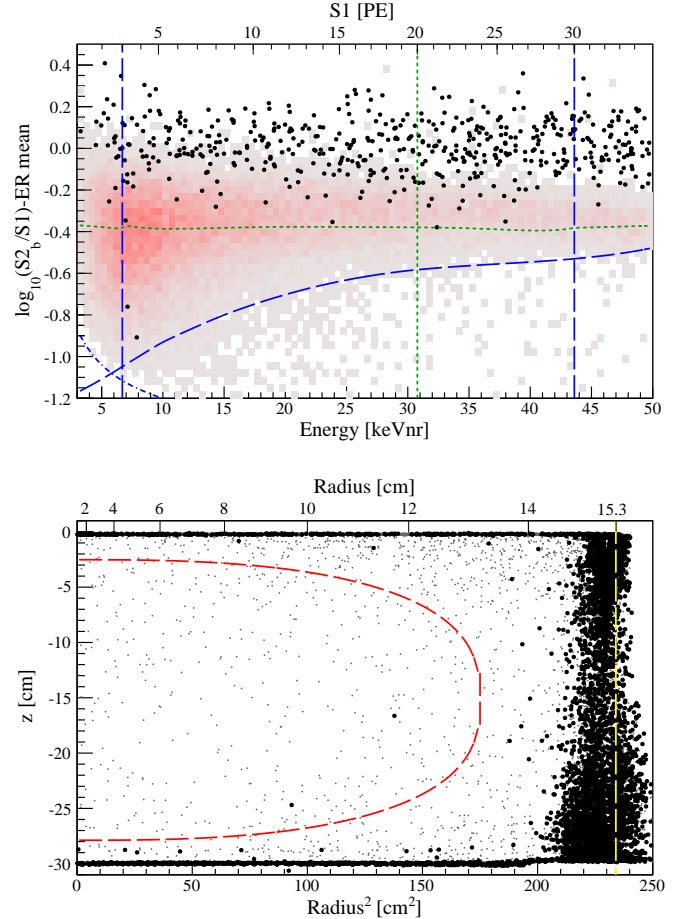


FIG. 2: (Top) Event distribution in the discrimination parameter space $\log_{10}(S2_b/S1)$, flattened by subtracting the distribution's mean, as observed after unblinding using all analysis cuts and a 34 kg fiducial volume (black points). A lower analysis threshold of 6.6 keV_{nr} (NR equivalent energy scale) is employed. The PL analysis uses an upper energy threshold of 43.3 keV_{nr} (3–30 PE) and the benchmark WIMP search region is limited to 30.5 keV_{nr} (3–20 PE). The negligible impact of the $S2 > 150$ PE threshold cut is indicated by the dashed-dotted blue line and the signal region is restricted by a lower border running along the 97% NR quantile. An additional hard $S2_b/S1$ discrimination cut at 99.75% ER rejection defines the benchmark WIMP search region from above (dotted green) but is only used to cross check the PL inference. The histogram in red indicates the NR band from the neutron calibration. Two events fall into the benchmark region where (1.0 ± 0.2) are expected from background. (Bottom) Spatial event distribution inside the TPC using a 6.6–43.3 keV_{nr} energy window. The 34 kg fiducial volume is indicated by the red dashed line. Gray points are above the 99.75% rejection line, black dots fall below.

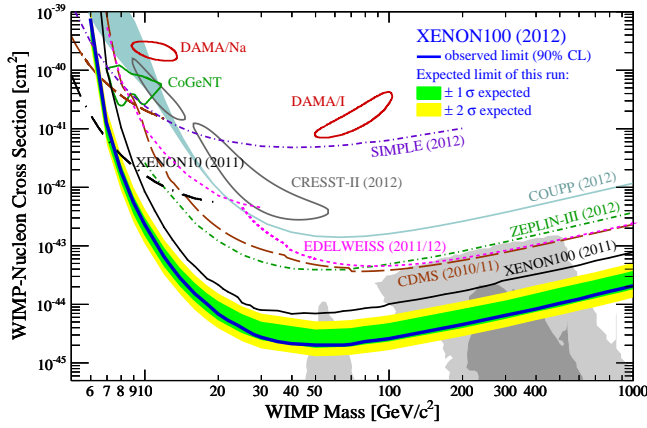


FIG. 3: New result on spin-independent WIMP-nucleon scattering from XENON100: The expected sensitivity of this run is shown by the green/yellow band ($1\sigma/2\sigma$) and the resulting exclusion limit (90% CL) in blue. For comparison, other experimental results are also shown [19–22], together with the regions ($1\sigma/2\sigma$) preferred by supersymmetric (CMSSM) models [18].

the benchmark region fluctuates to 2 events is 26.4% and confirms this conclusion.

A 90% confidence level exclusion limit for spin-independent WIMP-nucleon cross sections σ_χ is calculated, assuming an isothermal WIMP halo with a local density of $\rho_\chi = 0.3 \text{ GeV}/c^3$, a local circular velocity of $v_0 = 220 \text{ km/s}$, and a Galactic escape velocity of $v_{\text{esc}} = 544 \text{ km/s}$ [17]. Systematic uncertainties in the energy scale as described by the \mathcal{L}_{eff} parametrization of [6] and in the background expectation are profiled out and represented in the limit. Poisson fluctuations in the number of PEs dominate the S1 energy resolution and are also taken into account along with the single PE resolution. The expected sensitivity of this dataset in absence of any signal is shown by the green/yellow ($1\sigma/2\sigma$) band in Fig. 3. The new limit is represented by the thick blue line. It excludes a large fraction of previously unexplored parameter space, including regions preferred by scans of the constrained supersymmetric parameter space [18].

The new XENON100 data provide the most stringent limit for $m_\chi > 8 \text{ GeV}/c^2$ with a minimum of $\sigma = 2.0 \times 10^{-45} \text{ cm}^2$ at $m_\chi = 55 \text{ GeV}/c^2$. The maximum gap analysis uses an acceptance-corrected exposure of $2323.7 \text{ kg} \times \text{days}$ (weighted with the spectrum of a $100 \text{ GeV}/c^2$ WIMP) and yields a result which agrees with the result of Fig. 3 within the known systematic differences. The new XENON100 result continues to challenge the interpretation of the DAMA [19], CoGeNT [20], and CRESST-II [21] results as being due to scalar WIMP-nucleon interactions.

We acknowledge support from NSF, DOE, SNF, UZH, Volkswagen Foundation, FCT, Région des Pays de la Loire, STCSM, NSFC, DFG, Stichting FOM, Weizmann Institute of Science, and the friends of Weizmann Institute in memory of Richard Kronstein. We are grateful to LNGS for hosting and supporting XENON.

* Electronic address: ajmelgarejo@astro.columbia.edu

† Electronic address: marc.schumann@physik.uzh.ch

- [1] N. Jarosik et al., *Astrophys. J. Suppl.* **192**, 14 (2011); K. Nakamura et al. (PDG), *J. Phys.* **G37**, 075021 (2010).
- [2] G. Steigman and M. S. Turner, *Nucl. Phys.* **B253**, 375 (1985); G. Jungman, M. Kamionkowski, and K. Griest, *Phys. Rept.* **267**, 195 (1996).
- [3] G. Bertone, D. Hooper, and J. Silk, *Phys. Rept.* **405**, 279 (2005).
- [4] M. W. Goodman and E. Witten, *Phys. Rev.* **D31**, 3059 (1985).
- [5] E. Aprile et al. (XENON100), *Astropart. Phys.* **35**, 573 (2012).
- [6] E. Aprile et al. (XENON100), *Phys. Rev. Lett.* **107**, 131302 (2011).
- [7] M. Aglietta et al. (LVD), *Phys. Rev.* **D58**, 092005 (1998).
- [8] E. Aprile et al. (XENON100) *Astropart. Phys.* **35**, 43 (2011).
- [9] E. Aprile et al., *Phys. Rev.* **C79**, 045807 (2009).
- [10] X. Du et al., *Rev. Sci. Instr.* **75**, 3224 (2004).
- [11] E. Aprile et al. (XENON100), (2012), [arXiv:1207.3458](https://arxiv.org/abs/1207.3458).
- [12] E. Aprile et al. (XENON100), *Phys. Rev.* **D84**, 052003 (2011).
- [13] S. Yellin, *Phys. Rev.* **D66**, 032005 (2002).
- [14] G. Plante et al., *Phys. Rev.* **C84**, 045805 (2011).
- [15] E. Aprile et al., *Phys. Rev. Lett.* **97**, 081302 (2006).
- [16] M. M. Szydagis et al., *JINST* **6**, P10002 (2011).
- [17] M. C. Smith et al., *Mon. Not. R. Astron. Soc.* **379**, 755 (2007).
- [18] Combined region using C. Stenge et al., *JCAP* **1203**, 030 (2012); A. Fowlie et al. (2012), [arXiv:1206.0264](https://arxiv.org/abs/1206.0264); O. Buchmueller et al. (2011), [arXiv:1112.3564](https://arxiv.org/abs/1112.3564).
- [19] C. Savage et al., *JCAP* **0904**, 010 (2009).
- [20] C. E. Aalseth et al. (CoGeNT), *Phys. Rev. Lett.* **106**, 131301 (2011).
- [21] G. Angloher et al. (CRESST-II), *Eur. Phys. J.* **C72**, 1971 (2012).
- [22] Z. Ahmed et al. (CDMS), *Science* **327**, 1619 (2010); Z. Ahmed et al. (CDMS), *Phys. Rev. Lett.* **106**, 131302 (2011); E. Armengaud et al. (EDELWEISS), *Phys. Lett. B* **702**, 329 (2011); J. Angle et al. (XENON10), *Phys. Rev. Lett.* **107**, 051301 (2011); M. Felizardo et al. (SIMPLE), *Phys. Rev. Lett.* **108**, 201302 (2012); E. Behnke et al. (COUPP) (2012), [arXiv:1204.3094](https://arxiv.org/abs/1204.3094); D. Y. Akimov et al. (ZEPLIN-III), *Phys. Lett. B* **709**, 14 (2012); E. Armengaud et al. (EDELWEISS) (2012), [arXiv:1207.1815](https://arxiv.org/abs/1207.1815).